Analysis of stress effect on Lamb wave propagation in isotropic plates

C.T. Ng
School of Civil, Environmental & Mining Engineering, The University of Adelaide, SA 5005, Australia

M. Mohabuth & A. Kotousov
School of Mechanical Engineering, The University of Adelaide, SA 5005, Australia

ABSTRACT: This paper presents an analysis of the stress effect on Lamb wave propagation in isotropic plates based on the theory of nonlinear elasticity. In this study the plates are assumed to be initially isotropic hyperelastic and subjected to homogeneous stress. The theory of small deformations superimposed on large deformations is used to derive the acoustoelastic dispersion equations for both symmetric and anti-symmetric modes of Lamb waves. Different magnitudes of the inhomogeneous stress are considered in this study. The results of the theoretical predications show that the acoustoelastic effect of isotropy plates subjected to a realistic level of applied stresses is quite significant, especially for higher order Lamb wave modes near the cut-off frequencies.

1 INTRODUCTION

The use of guided waves for structural health monitoring (SHM) has been widely recongised as one of the promising technologies in different engineering fields, e.g. civil, mechanical and aerospace engineering. A number of safety inspection techniques (Giurgiutiu & Bao 2004; Croxford et al. 2007; Veidt et al. 2008; Ng 2014b; Vanli & Jun 2014) have been developed to enhance the safety and increase the sustainability of the structures. In general guided wave can propagate in different types of structures. Based on the propagation characteristics, research works have focused on one-dimensional waveguides, e.g. rods, beams and pipes (Rucka 2010; Ng 2014a; Leinvo et al. 2015), and two-dimensional waveguides, e.g. plates and shells (Giurgiutiu & Bao 2004; Kudela et al. 2007; Ng 2015b).

Guided waves propagate in thin plates refer to Lamb waves. The fundamental symmetric (S_0) and anti-symmetric modes (A_0) of Lamb wave are the two most commonly used wave modes in damage detection. Most of the Lamb wave based damage detection techniques operate below the cut-off frequency of the higher order Lamb wave modes (Ihn & Chang 2008; Ng *et al*. 2009; Rose & Wang 2010; Aryan et al. 2016). This can limit the generated wave modes to only the S_0 and A_0 Lamb waves, and hence, simplifying the data interpretation in the damage detection process. At low-frequency regime (i.e. below the cut-off frequency), S_0 Lamb wave is non-dispersive, and hence, it has a much longer propagation distance compared to the A_0. However, the A_0 Lamb wave is more sensitive to damages with smaller sizes as its wavelength is shorter than that of the S_0 Lamb wave (He & Ng 2015).

In general most the Lamb wave based SHM systems rely on a transducer network with permanently installed transducers, such as surface bonded or embedded transducers, to cover a pre-defined inspection area on a structure (Sohn *et al*. 2004; Su & Ye 2004; Ng 2015a). Each of the transducers can act as both actuator and sensor for excitation and measurement of Lamb waves. The damage detection is usually carried out by comparing the current measurements with the Lamb wave signals measured at pristine condition of the structure (baseline measurements). One of the commonly used approaches to extract the scattered wave information from the measured Lamb wave signals is to subtract the current measurements from the baseline measurements, i.e. baseline subtraction (Lee *et al*. 2011; Ng 2015a).

In the literature it was shown that the variation of the environmental conditions, i.e. variation of temperature and applied loads, could make the baseline subtraction fail. Konstantinidis *et al*. (2006) investigated the temperature stability of guided wave damage detection based on the baseline subtraction approach. They demonstrated that the change in temperature could cause significant errors in the baseline subtraction, and make the guided wave based damage detection techniques fail in detecting damages. Chen & Wilcox (2007) presented a study of the effect of loads on the guided wave propagation. Their study showed that the applied load could

change the phase and group velocity of the guided wave.

In practical situation the variation of the temperature and applied load are unavoidable in long-term SHM using the guided wave approach. Therefore, it is important to gain physical insights into the effect of stress variation on the Lamb wave propagation. This can provide a basis in developing an effective strategy to compensate the effect of stress variation on damage detection, which is essential for industrial deployment of the guided wave SHM system. The objective of this study is to investigate the effect of homogeneous stress on the propagation of Lamb waves in an initially isotropic hyperelastic plate. The dispersion equations for Lamb wave propagation in pre-stressed the plate are derived based on the theory of acoustoelasticity.

This paper is structured as follows. The constitutive equation for an isotropic hyperelastic material with initial stress and the equation governing incremental deformations superimposed on a finite deformation are reviewed. A specialised form of the strain energy function, which accounts for weakly nonlinear elasticity, is then derived. The governing equations and the selected form of the energy function are used to obtain the dispersion equations for Lamb wave propagation in the pre-stressed plates. Several examples of the effect of uniaxial homogeneous stress on the propagation of Lamb waves in plates are then provided. Conclusions are drawn at the end of the paper.

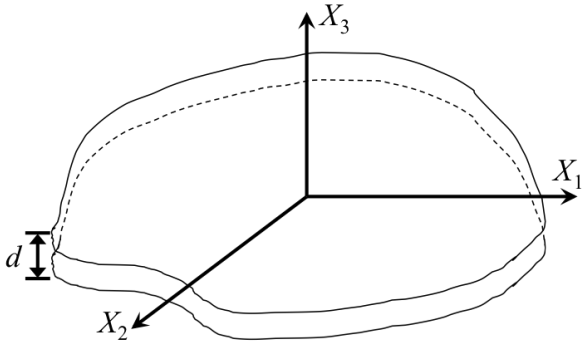

Figure 1. Reference coordinate system

2 THEORY OF ACOUSTOELASTICITY

2.1 *Governing equations*

We first consider an isotropic hyperelastic plate with thickness d and density ρ_r at stress-free reference condition and a reference Cartesian coordinate system $\mathbf{X} = (X_1, X_2, X_3)$ at the mid-plane of the plate as shown in Figure 1. When the plate subjected to a general homogeneous deformation, the coordinate of the material points after the deformation can be defined as $\mathbf{x} = (x_1, x_2, x_3)$ and it can be related to the reference Cartesian coordinate system as

$$\mathbf{x} = \mathbf{F}\mathbf{X} \tag{1}$$

where $\mathbf{F} = diag[\lambda_1, \lambda_2, \lambda_3]$ is the deformation gradient tensor. λ_1 λ_2 and λ_3 are the principal stretches of the deformation.

For an unconstrained material, the nominal and Cauchy stress tensors are given by

$$\mathbf{S} = \frac{\partial W}{\partial \mathbf{F}}, \quad \boldsymbol{\sigma} = J^{-1}\mathbf{F}\frac{\partial W}{\partial \mathbf{F}} \tag{2}$$

where $W = W(\mathbf{F})$ is the strain-energy function and $J = \det \mathbf{F}$. We then consider the superposition of a small-amplitude time-dependent motion $\mathbf{u}(\mathbf{x}, t)$ upon the static finite deformation. The material response due to this incremental deformation can be described by the incremental constitutive relation (Destrade & Ogden 2013)

$$\dot{S}_{0pi} = A_{0piqj}\frac{\partial u_j}{\partial x_q} \tag{3}$$

where $\dot{S}_0$ is the incremental nominal stress tensor. The incremental equations of motions are given by

$$A_{0piqj}\frac{\partial^2 u_j}{\partial x_p \partial x_q} = \rho\frac{\partial^2 u_i}{\partial t^2} \tag{4}$$

where $\rho = \rho_r J^{-1}$ is the density of the material after the deformation. A_{0piqj} is the components of the elasticity tensor and can be expressed in terms of the strain energy function W as

$$A_{0piqj} = J^{-1}F_{pa}F_{qb}\frac{\partial^2 W}{\partial F_{ia}\partial F_{jb}} \tag{5}$$

with $A_{opiqi} = A_{0qjpi}$ (Destrade & Ogden 2013).

2.2 *Weakly nonlinear elasticity*

The strain energy function W is specialized to weakly nonlinear elasticity for studying small but finite elastic effects. The strain energy function W can be expressed in a form similar to Murnaghan's expansion and in terms of the principal invariant (Murnaghan 1937; Destrade & Ogden 2013) as

$$\begin{aligned} W = {} & \frac{\lambda_0}{8}(I_1 - 3)^2 + \frac{\mu}{4}(I_1^2 - 2I_1 - 2I_2 + 3) + \\ & \frac{l}{24}(I_1 - 3)^3 + \frac{m}{12}(I_1 - 3)(I_1^2 - 3I_2) + \\ & \frac{n}{8}(I_1 - I_2 + I_3 - 1) \end{aligned} \tag{6}$$

where λ_0 and μ are the classical Lamé constants. l, m, n are the third order elastic constants. I_1, I_2 and I_3 are the principal invariants and are defined as

$$\begin{aligned} I_1 &= \lambda_1^2 + \lambda_2^2 + \lambda_3^2 \\ I_2 &= \lambda_2^2\lambda_3^2 + \lambda_3^2\lambda_1^2 + \lambda_1^2\lambda_2^2 \\ I_3 &= \lambda_1^2\lambda_2^2\lambda_3^2 \end{aligned} \tag{7}$$

The components of the elasticity tensor are given by

$$\begin{aligned} JA_{0piqj} &= 2\left(W_1 + I_1 W_2\right) B_{pq}\delta_{ij} + \\ &2W_2\left(2B_{pi}B_{qj} - B_{iq}B_{jp} - B_{pr}B_{rq}\delta_{ij} - B_{pq}B_{ij}\right) + \\ &2I_3 W_3\left(2\delta_{ip}\delta_{jq} - \delta_{iq}\delta_{jp}\right) + 4W_{11}B_{ip}B_{jq} + \\ &4W_{12}\left(2I_1 B_{ip}B_{jq} - B_{ip}B_{jr}B_{rq} - B_{jq}B_{ir}B_{rp}\right) \end{aligned} \tag{8}$$

where the coefficients W_1, W_2, W_3, W_{11} and W_{12} can be obtained from Equation (6). B_{ij} are the components of the left Cauchy-Green deformation tensor $\mathbf{B} = \mathbf{F}\mathbf{F}^T$. δ_{ij} is the Kronecker delta.

2.3 *Uniform extension with lateral contraction*

Considering the plate subjected to a uniaxial load and deformed finitely, the uniaxial Cauchy stress σ can be taken to be along the $\mathbf{e}_1$ direction. Hence, $\sigma_{11} = \sigma$, $\sigma_{22} = \sigma_{33} = 0$ and the corresponding principal stretch is λ_1. There is symmetry perpendicular to the $\mathbf{e}_1$ axis as the plate was initially isotropic and without pre-stress, and hence, $\lambda_2 = \lambda_3$ (Ogden 1984). The uniform extension is specified in terms of the nominal stress tensor, which provides relation between the axial force of the deformed condition to the area in the reference (undeformed) condition. The principal components of the nominal stress can be expressed in terms of the principal stretches as

$$S_{ii} = \frac{\partial W}{\partial \lambda_i} \tag{9}$$

For a given uniaxial stress field S_{11}, the principal stretches can be determined by inverting the relation in Equation (9) with $S_{22} = S_{33} = 0$. The principal Cauchy stresses and the components of the elasticity tensor can be obtained using Equations (2) and (8), respectively. It should be noted that the uniaxial stress field leads to strain induced anisotropic, and hence, the elastic response of the plate becomes transversely isotropic in nature. However, the elasticity tensor does not process the same symmetry as in the case of classical transversely isotropic linear elasticity (Destrade & Ogden 2013).

3 ACOUSTOELASTIC LAMB WAVES

To describe the propagation of acoustoelastic Lamb waves in a plate subjected to the homogeneous uniaxial stress field, it requires the equation governing incremental motions superimposed on a finite deformation, i.e. Equation (4), to be solved in conjunction with stress-free boundary conditions at the surfaces of the plate. Assuming the waves only propagates along the direction of the applied uniaxial stress and they are planes waves of the form

$$u_j = U_j e^{ik(x_1 + ax_3 - ct)}, \quad j = 1,2,3 \tag{10}$$

where u_j and U_j are the particle displacement and amplitude of the displacement, respectively. k is the wavenumber along the x_1 direction. a is the ratio of the wavenumbers in the x_3 direction to that in the x_1 direction. c is the phase velocity in the x_1 direction.

Substituting Equation (10) into Equation (4) yields an eigenvalue problem as

$$K_{ij}(a)u_j = 0, \quad i,j = 1,2,3 \tag{11}$$

We assume the wave only propagates along the direction of applied stress and the elasticity tensor is refereed to the principal axes of the pre-strain. Therefore, the only non-zero components of the elasticity tensor for a pre-stressed isotropic material are A_{0iiii}, A_{0iijj}, A_{0ijij} and A_{0ijji} for $i \neq j$ (Ogden 1984), and hence, $K_{12} = K_{21} = K_{23} + K_{32} = 0$ and the non-zero components of K_{ij} are

$$\begin{aligned} K_{11} &= \rho c^2 - A_{01111} - A_{03131}a^2 \\ K_{13} &= -a\left(A_{01133} + A_{03113}\right) \\ K_{22} &= \rho c^2 - A_{01212} - A_{03232}a^2 \\ K_{31} &= -a\left(A_{01331} + A_{03311}\right) \\ K_{33} &= \rho c^2 - A_{01313} - A_{03333}a^2 \end{aligned} \tag{12}$$

Since $K_{12} = K_{21} = K_{23} + K_{32} = 0$, it means that the analysis can be confined to displacements in x_1 and x_3 direction only as the shear horizontal wave motions uncouple from the Lamb wave motion (Nayfeh & Chimenti 1989). The eigenvalue problem in Equation (11) can be reduced to

$$K_{ij}(a)u_j = 0, \quad i,j \in \{1,3\} \tag{13}$$

Since the eigenvalue problem has non-trivial solutions, $|K_{ij}| = 0$, $i,j \in \{1,3\}$. This yields a fourth order equation as

$$\Gamma_1 a^4 + \Gamma_2 a^2 + \Gamma_3 = 0 \tag{14}$$

where Γ_1, Γ_2 and Γ_3 are given by

$$\Gamma_1 = A_{03131}A_{03333} \tag{15}$$

$$\begin{aligned} \Gamma_2 = &-\rho c^2\left(A_{03333} + A_{03131}\right) + A_{03333}A_{01111} + \\ &A_{03131}A_{01313} - A_{01133}A_{01331} \end{aligned} \tag{16}$$

$$\Gamma_3 = \rho^2 c^4 - \rho c^2\left(A_{01313} + A_{01111}\right) + A_{01111}A_{01313} \tag{17}$$

The fourth order equation can be further reduced to a quadratic equation in term of a^2. This results in four solutions for a denoted by a_q for $q \in \{1,2,3,4\}$ with $a_2 = -a_1$ and $a_4 = -a_3$.

Using Equation (12), we define the displacement ratio of U_3 to U_1 for each of the four values of a as R_q and it can be expressed as

$$W_q = \frac{\left(\rho c^2 - A_{01111} - A_{03131} a_q^2\right)}{a_q \left(A_{01133} + A_{03113}\right)} \tag{18}$$

Using the principle of superposition, Equation (18) allows the displacement field u_1 and u_3 of the Lamb waves to be written in term of the displacement ratio R_q as

$$\begin{aligned} u_1 &= \sum_{q=1}^{4} U_1 a_q e^{ik\left(x_1 + a_q x_3 - ct\right)} \\ u_3 &= \sum_{q=1}^{4} U_1 a_q W_q e^{ik\left(x_1 + a_q x_3 - ct\right)} \end{aligned} \tag{19}$$

and the stress field can be found by substituting Equation (19) into Equation (3) as

$$\begin{aligned} \dot{S}_{033} &= \sum_{q=1}^{4} ikD_{1q} U_1 a_q e^{ik\left(x_1 + a_q x_3 - ct\right)} \\ \dot{S}_{013} &= \sum_{q=1}^{4} ikD_{2q} U_1 a_q W_q e^{ik\left(x_1 + a_q x_3 - ct\right)} \end{aligned} \tag{20}$$

where

$$\begin{aligned} D_{1q} &= A_{03311} + a_q A_{03333} W_q \\ D_{2q} &= A_{01313} a_q + A_{01331} W_q \end{aligned} \tag{21}$$

To account the relations $a_2 = -a_1$ and $a_4 = -a_3$ in Equations (18) - (21), it results in the following restrictions

$$\begin{aligned} W_{j+1} &= -W_j \\ D_{1j+1} &= D_{1j} \qquad \text{for } j = 1, 3 \\ D_{2j+1} &= -D_{2j} \end{aligned} \tag{22}$$

To satisfy conditions of Lamb wave, i.e. the incremental traction free boundary conditions at the upper and lower surfaces of the plate, the components of the incremental nominal stress become

$$\dot{S}_{033} = \dot{S}_{013} = 0 \quad \text{at } x_3 = \pm\frac{d}{2} \tag{23}$$

This leads to the following four equations

$$ik \begin{bmatrix} D_{11}E_1 & D_{12}E_2 & D_{13}E_3 & D_{14}E_4 \\ D_{21}E_1 & D_{22}E_2 & D_{23}E_3 & D_{24}E_4 \\ D_{11}\bar{E}_1 & D_{12}\bar{E}_2 & D_{13}\bar{E}_3 & D_{14}\bar{E}_4 \\ D_{21}\bar{E}_1 & D_{22}\bar{E}_2 & D_{23}\bar{E}_3 & D_{24}\bar{E}_4 \end{bmatrix} \begin{bmatrix} U_{11} \\ U_{12} \\ U_{13} \\ U_{14} \end{bmatrix} e^{ik\left(x_1 - ct\right)} = 0 \tag{24}$$

where $U_{1q} = U_1 a_q$, $E_q = e^{ika_q(d/2)}$ and $\bar{E}_q = e^{-ika_q(d/2)}$. As Equation (24) has non-trivial solutions, the determinant of the coefficient matrix in Equation (24) is equal to zero.

$$\begin{vmatrix} D_{11}E_1 & D_{12}E_2 & D_{13}E_3 & D_{14}E_4 \\ D_{21}E_1 & D_{22}E_2 & D_{23}E_3 & D_{24}E_4 \\ D_{11}\bar{E}_1 & D_{12}\bar{E}_2 & D_{13}\bar{E}_3 & D_{14}\bar{E}_4 \\ D_{21}\bar{E}_1 & D_{22}\bar{E}_2 & D_{23}\bar{E}_3 & D_{24}\bar{E}_4 \end{vmatrix} = 0 \tag{25}$$

Using Equation (22), Equation (25) can be further reduced to two characteristic equations as

$$\begin{aligned} D_{11}D_{23}\cot\left(\gamma\alpha_1\right) - D_{13}D_{21}\cot\left(\gamma\alpha_3\right) &= 0 \\ D_{11}D_{23}\tan\left(\gamma\alpha_1\right) - D_{13}D_{21}\tan\left(\gamma\alpha_3\right) &= 0 \end{aligned} \tag{26}$$

for the symmetric and anti-symmetric Lamb wave modes, respectively. $\gamma = kd/2 = \omega d/2c$. ω is the angular frequency of the wave. The dispersion curves can be obtained by solving Equation (26) using numerical methods (Gandhi 2010).

4 EFFECT OF APPLIED STRESS ON LAMB WAVE PROPAGATION

This section investigates the effect of the applied stress on dispersion curves of symmetric and anti-symmetric Lamb wave modes obtained using Equation (26). We consider a 6061-T6 aluminium plate with the elastic properties shown in Table 1, which were obtained from the experimental work of Asay and Guenther (1967).

Table 1. Elastic properties for 6061-T6 aluminum

λ_0	54.3GPa
μ	27.2GPa
l	-281.5GPa
m	-339.0GPa
n	-416.0GPa
ρ	2704 kg/m^3

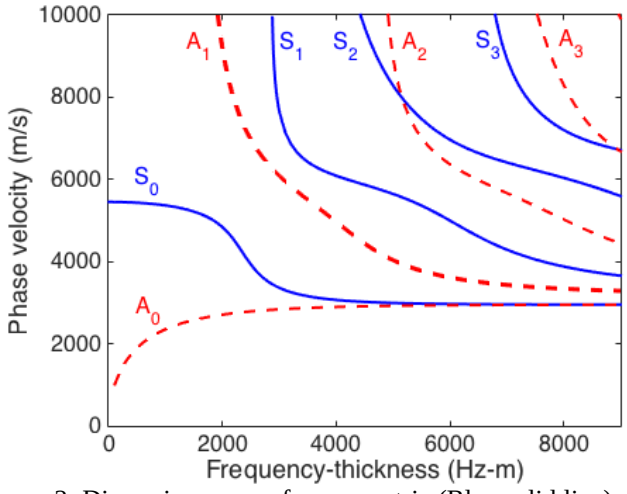

Figure 2. Dispersion curves for symmetric (Blue solid line) and anti-symmetric (red dashed line) mode of Lamb waves propagating in a 6061-T6 aluminum plate along the direction of a uniaxial applied stress of 100 MPa.

As an example Figure 2 shows the phase velocity dispersion curves for symmetric and anti-symmetric modes of Lamb waves subjected to a uniaxial tension of 100 MPa. The propagation of the waves is along the direction of a uniaxial applied stress. It should be noted that as the shear horizontal modes are decoupled from the Lamb wave modes, they are not shown in Figure 2.

To investigate the effect of the uniaxial tension on the Lamb wave propagation, Figures 3a, 3b and 3c show the change of phase velocity Δc for S_0, S_1 and S_2 Lamb waves at 20 MPa, 40 MPa, 60 MPa and 80 MPa applied uniaxial tensions, respectively. As shown in Figure 3, the change in the phase velocity is negative for all considered symmetric modes, which means the tensile stress reduces the phase velocity. This is consistent with the findings that bulk wave speed along the direction of an applied tensile load is less than the unstressed wave speed (Hughes & Kelly 1953). Figure 3 also shows that the change of the phase velocity increases with the applied uniaxial tensile stress at the lower frequency-thickness region.

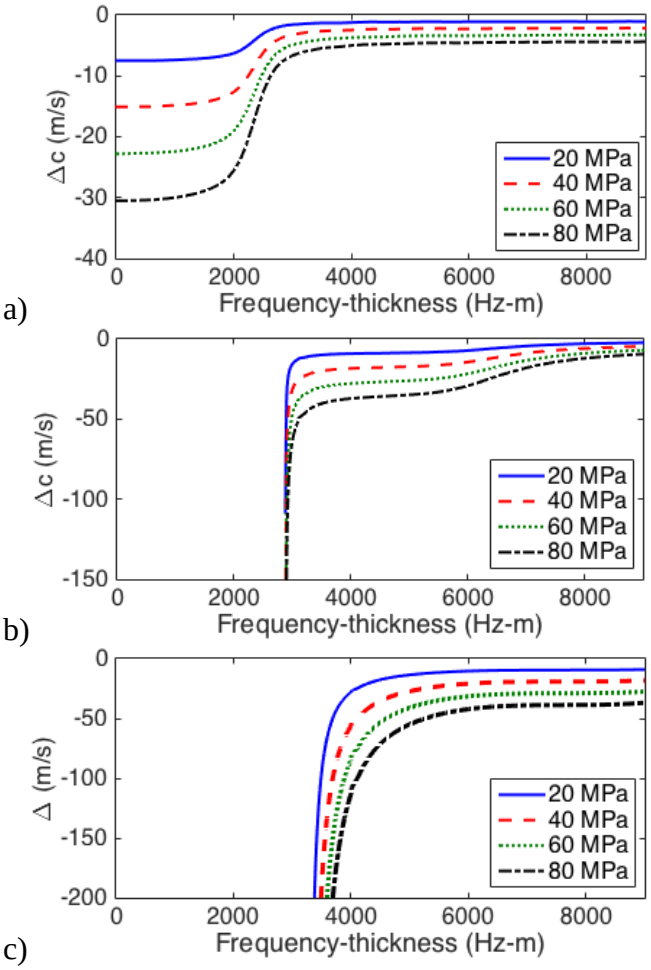

Figure 3. Change of phase velocity for S_0, S_1 and S_2 Lamb wave at different values of uniaxial tension

Figure 4 shows the change of the phase velocity for A_0, A_1 and A_2 Lamb waves. As shown in Figure 4a, the change of the phase velocity of A_0 Lamb wave at the very low frequency-thickness region is positive but it becomes negative for larger value of frequency-thickness. Similar to the symmetric modes of Lamb waves, the tensile stress leads to negative values in the change of the phase velocity for A_1 and A_2 Lamb waves. In general the results shown in Figures 3 and 4 indicate that the higher order wave modes have better sensitivity to the applied uniaxial tensile stress.

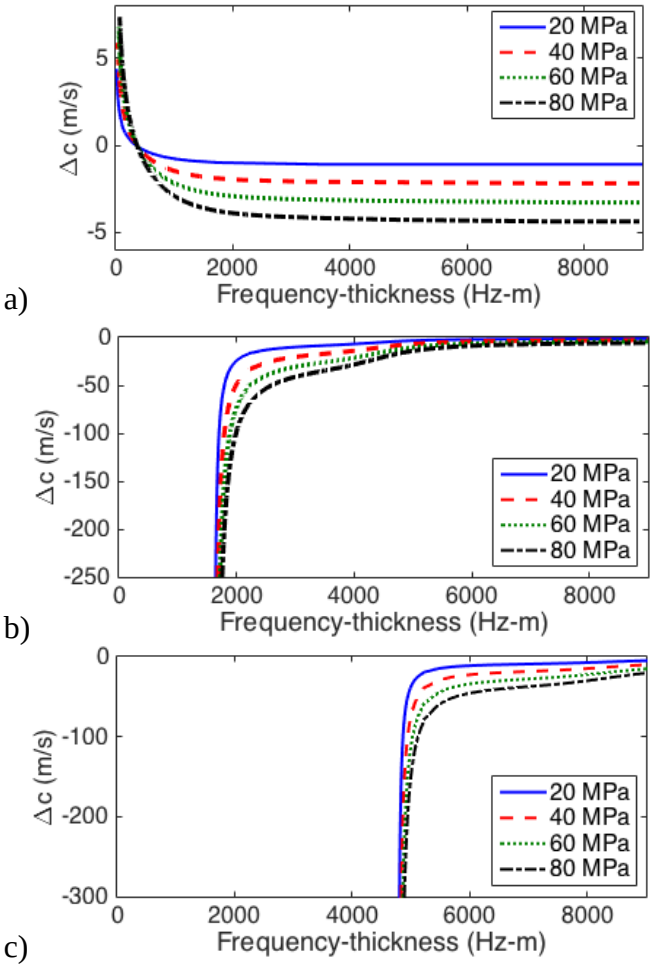

Figure 4. Change of phase velocity for A_0, A_1 and A_2 mode Lamb wave at different values of uniaxial tension

5 CONCLUSIONS

This study has investigated the effect of applied stress on the Lamb wave propagation in initially isotropic elastic plates. It is assumed that the plates are subjected to a homogeneous stress field. The governing equations of motion and dispersion equations have been derived based on the nonlinear theory of elasticity and the invariant-based formulation of the strain energy function.

The results predicted by the derived equations have shown that the phase velocity of Lamb wave generally decreases with the magnitude of the applied uniaxial tensile stress. The low frequency-thickness region and higher order modes of Lamb waves have higher sensitivity to the applied uniaxial tensile stress. Overall this study has provided a theoretical basis to take into account the effect of the ap-

plied stress in using the Lamb waves for damage detection.

6 ACKNOWLEDGEMENTS

The project was supported by Department of Further Education, Employment, Science & Technology, Government of South Australia, and Australian Research Council under Catalyst Research Grant Program and DP160102233, respectively. The supports are greatly appreciated.

7 REFERENCES

Aryan, P., Kotousov, A., Ng, C.T. & Cazzolato, B. 2016. A model-based method for damage detection with guided wave. *Structural Control and Health Monitoring*. DOI: 10.1002/stc.1884.

Asay, J.R. & Guenther, A.H. 1967. Ultrasonic studies of 1060 and 6061-T6 aluminum. *Journal of Applied Physics* 38: 4086-4088.

Chen, F. & Wilcox, P.D. 2007. The effect of load on guided wave propagation. *Ultrasonics* 47(1-4): 111-122.

Croxford, A.J., Wilcox, P.D., Drinkwater, B.W. & Konstantinidis, G. 2007. Strategies for guided-wave structural health monitoring. *Proceedings of the Royal Society* 463: 2961-2981.

Destrade, M. & Ogden, R.W. 2013. On stress-dependent elastic moduli and wave speeds. *IMA Journal of Applied Mathematics* 78(5): 965-997.

Flynn, E.B., Todd, M.D., Croxford, A.J., Drinkwater, B.W. & Wilcox, P.D. 2012. Enhanced detection through low-order stochastic modeling for guided-wave structural health monitoring. *Structural Health Monitoring* 11(2): 149-160.

Gandhi, N. 2010. *Determination of dispersion curves for acoustoelastic Lamb wave propagation*. Master Thesis, Georgia Institute of Technology, USA.

Giurgiutiu, V. & Bao, J.J. 2004. Embedded-ultrasonic structural radar for in situ structural health monitoring of thin-wall structures. *Structural Health monitoring* 121: 121-140

He, S. & Ng, C.T. 2015. Analysis of mode conversion and scattering of guided waves at cracks in isotropic beams using a time-domain spectral finite element method. *Electronic Journal of Structural Engineering* 14(1): 20-32.

Hughes, D.S. & Kelly, J.L. 1953. Second-order elastic deformation of solids. *Physical Review* 92(5): 1145-1149.

Ihn, J.B. & Chang, F.K. 2008. Pitch-catch active sensing methods in structural health monitoring or aircraft structures. *Structural Health Monitoring* 7(1): 5-19.

Konstantinidis, G., Drinkwater, B.W. & Wilcox, P.D. 2006. The temperature stability of guided wave structural health monitoring systems. *Smart Materials and Structures* 15(4): 967-976.

Kudela, P., Zak, A., Krawczuk, M. & Ostachowicz, W. 2007. Modelling of wave propagation in composite plates using the time domain spectral element method. *Journal of Sound and Vibration* 302: 728-745.

Lee, J.S., Park, G., Kim, C.G. & Farrar, C. 2011. Use of relative baseline features of guided waves for in situ structural health monitoring. *Journal of Intelligent Material Systems and Structure* 22(2): 175-189.

Leinov, E., Lowe, M.J.S. & Cawley, P. 2015. Investigation of guided wave propagation and attenuation in pipe buried in sand. *Journal of Sound and Vibration* 347: 96-114.

Murnaghan, F.D. 1937. Finite deformations of an elastic solid. *American Journal of Mathematics* 59(2): 235-260.

Nayfeh, A.H. & Chimenti, D.E. 1989. Free wave propagation in plates of general anisotropic media. *Journal of Applied Mechanics* 56: 881-886.

Ng, C.T. 2014a. Bayesian model updating approach for experimental identification of damage in beams using guided wave. *Structural Health Monitoring* 13(4): 359-373.

Ng, C.T. 2014b. On the selection of advanced signal processing techniques for guided wave damage identification using a statistical approach. *Engineering Structures* 67: 50-60.

Ng, C.T. 2015a. A two-stage approach for quantitative damage imaging in metallic plates using Lamb waves. *Earthquake and Structures* 8(4): 821-841.

Ng, C.T. 2015b. On accuracy of analytical modeling of Lamb wave scattering at delaminations in multilayered isotropic plates. *International Journal of Structural Stability and Dynamics* 15(8): 1540010.

Ng, C.T., Veidt, M. & Rajic, M. 2009. Integrated piezoceramic transducers for imaging damage in composite laminates. *Proceedings of SPIE* 7493: 74932M.

Ogden, R.W. 1984. *Non-linear elastic deformations*, Ellis Horwood, Chichester.

Rose, L.R.F. & Wang, C.H. 2010. Mindlin plate theory for damage detection: imaging of flexural inhomogeneities. *Journal of the Acoustical Society of America* 127: 754-763.

Rucka, M. 2010. Experimental and numerical studies of guided wave damage detection in bars with structural discontinuities. *Archive of Applied Mechanics* 80(12): 1371-1390.

Sohn, H. Park, G., Wait, J.R., Limback, N.P. & Farrar, C.R. 2004. Wavelet-based active sensing for delamination detection in composite structures. *Smart Materials and Structures* 13: 153-160.

Su, Z. & Ye, L. 2004. Fundamental Lamb mode-based delamination detection for CF/EP composite laminates using distributed piezoelectric. *Structural Health Monitoring* 3(1): 43-68.

Vanli, O.A. & Jun, S. 2014. Statistical updating of finite element model with Lamb wave sensing data for damage detection problems. *Mechanical Systems and Signal Processing* 42(1-2): 137-151.

Veidt, M, Ng, C.T., Hames, S. & Wattinger, T. 2008. Imaging laminar damage in plates using Lamb wave beamforming. *Advanced Materials Research* 47-50: 666-669.